Solitons on nanotubes and fullerenes as solutions of a modified non-linear Schrödinger equation

Yves Brihaye[*]

Faculté des Sciences, Université de Mons-Hainaut, 7000 Mons, Belgium

Betti Hartmann[†]

School of Engineering and Sciences,

International University Bremen (IUB), 28725 Bremen, Germany

(Dated: February 5, 2008)

[*] Yves.Brihaye@umh.ac.be

[†] b.hartmann@iu-bremen.de

Abstract

Fullerenes and nanotubes consist of a large number of carbon atoms sitting on the sites of a regular lattice. For pratical reasons it is often useful to approximate the equations on this lattice in terms of the continuous equation. At the moment, the best candidate for such an equation is the modified non-linear Schrödinger equation. In this paper, we study the modified non-linear Schrödinger equation, which arises as continuous equation in a system describing an excitation on a hexagonal lattice. This latter system can e.g. describe electron-phonon interaction on fullerene related structures such as the buckminster fullerene and nanotubes. Solutions of this modified non-linear Schrödinger equation, which have solitonic character, can be constructed using an Ansatz for the wave function, which has time and azimuthal angle dependence introduced previously in the study of spinning boson stars and Q-balls. We study these solutions on a sphere, a disc and on a cylinder.

Our construction suggests that non-spinning as well as spinning solutions, which have a wave function with an arbitrary number of nodes, exist. We find that this property is closely related to the series of well-known mathematical functions, namely the Legendre functions when studying the equation on a sphere, the Bessel functions when studying the equation on a disc and the trigonometric functions, respectively, when studying the equation on a cylinder.

I. INTRODUCTION

Fullerenes and fullerene related structures have gained a lot of interest in the past 20 years. Fullerenes were discovered for the first time in 1985 [1] and are carbon-cage molecules with a large number n of carbon (C) atoms bonded in a nearly spherically symmetric configuration. The configuration is such that three of the valence electrons of the carbon atom form the bounds with the neighbouring carbon atoms. This means, that one "free" valence electron can "hop" along the the n positions in the fullerene.

The C_{60} fullerene, the so-called "buckminster" fullerene, has 60 carbon atoms arranged on a lattice with 20 hexagons and 12 pentagons. It has a diameter of $d_{60} \approx 7$ Å. In general, fullerenes with n carbon atoms consists of lattices with 12 pentagons and $(\frac{n}{2} - 10)$ hexagons, where $n \geq 24$ has to be even.

Fullerides are alkali-doped fullerenes, i.e. fullerenes on which alkali metal atoms such as rubidium (Rb), potassium (K), caesium (Cs) or sodium (Na) are put. These alkali metals donate one electron each. It was observed that such "doping" leads to a metallic or even superconducting behaviour [2]. The interesting thing about this is that the transition temperature T_c of the fullerides is quite high for superconductors, e.g. $T_c = 33$ K for a $RbCs_2C_{60}$ [3]. In an attempt to explain this high transition temperature, it was found that phonon-electron interactions in the fullerides can explain this phenomenon quite well [4].

Nanotubes are fullerene related structures, which were discovered for the first time in 1991 [5]. These molecules have cylindrical shape and the carbon atoms are arranged on a hexagonal grid. The ends of the nanotubes are typically closed by caps of pentagonal rings. While the tubes discovered in 1991 were multi-layered, single-walled tubes were synthesised in 1993 [6]. The tubes are distinguished by their chirality, diameter and lengths. They have average diameters of 1.2 to 1.4 nm and can be up to 2 mm long. Concerning their chirality, the tubes are typically put into three different classes: armchair, zigzag or chiral tubes [7]. Depending on their structure, the tubes have different mechanical, thermal, optical and electrical properties. The chirality determines e.g. whether the tubes behave metallic or semiconducting. These facts also lead to the conclusion that a distortion of the hexagonal lattice would influence the energy-band gap. A distortion can be achieved in two ways: either by external, mechanical forces such as bending, stretching or twisting or by an interaction of the lattice with an internal excitation. Trying to explain the dispersion-free energy transport

in biopolymers, Davydov realised [8] that the interaction of an internal excitation with the distorted lattice (whose distortion was initially caused by the internal excitation) leads to a localised state, a soliton [9]. For the case of biopolymers, the internal excitation is an amide I vibration.

Motivated by the research on fullerene related structures, the interaction of a 2-dimensional hexagonal lattice with an excitation caused by an "excess electron" was studied recently [10]. The Hamiltonian is of Fröhlich-type and describes "electron-phonon" interactions. It was found that the existence of soliton-like structures depends crucially on the value of the "electron-phonon" coupling.

Interestingly, in the continuum limit, this latter system of equations reduces to a modified non-linear Schrödinger equation, where the extra term appearing due to the discreteness of the lattice and the "electron-phonon" interaction, leads to the stabilisation of the soliton. The appearance of this type of equation has been observed also for a similar system on a quadratic lattice [11, 12]. Consequently, the modified non-linear Schrödinger equation was studied on a 2-dimensional plane in [13] and on a sphere in [14] using an Ansatz previously introduced in the study of boson stars [15] and Q-balls [16]. Non-spinning as well as spinning solutions with and without nodes were constructed.

In this paper, we study the modified non-linear Schrödinger equation arising as continuum limit of the equations describing the interaction of an electron-like excitation with a hexagonal lattice. In Section II, we review some generalities. Using the Ansatz introduced in [15, 16], we construct solutions for three different cases, which we describe in Sections III-V. In Section III, we discuss the results for the solutions on the sphere obtained in [14] from another point of view, namely we give the spectrum of the equation. In Section IV, we discuss the solutions on a 2-dimensional disc with fixed radius and demonstrate how the solutions obtained on the plane [13] can be understood in this context. In Section V, we discuss the equation on a cylinder with fixed radius and fixed length. We give our conclusions in Section VI.

II. THE MODIFIED NON-LINEAR SCHRÖDINGER EQUATION: GENERALI-TIES

The starting point is a coupled systems of discrete equations describing the interaction of an excitation (e.g. an "excess electron") with a regular lattice in two dimensions. The excitation is given in terms of a complex valued scalar field ψ, while the lattice displacements are described by two fields, one standing for the displacement in x, the other for that in y direction. These discrete equations were studied for the quadratic lattice in [11, 12] and for the hexagonal lattice in [10]. Remarkably, it was found for the hexagonal lattice that in the stationary limit it is possible to replace the full system of equation, in which the excitation field ψ and the displacement fields are coupled, by a modified discrete non-linear Schrödinger equation. This is not possible for the quadratic lattice.

In the continuum limit, both systems of equations reduce to a modified non-linear Schrödinger equation. The new term appearing in this equation, which results from both the discreteness of the lattice as well as from the interaction between the lattice and the complex valued scalar field ψ ("lattice-excitation interaction"), leads to the stabilisation of the solution. The difference between the quadratic and the hexagonal case is just the coefficient in front of the non-linear term in the equation, which, however is of the same order of magnitude for the two cases.

Since we are dealing with fullerene related structures here, we consider the modified non-linear Schrödinger equation, which arises as continuum limit in the hexagonal case [10, 13]. In dimensionless variables it reads:

$$i\frac{\partial \psi}{\partial t} + \Delta \psi + 4g\psi \left(|\psi|^2 + \frac{1}{8}\Delta |\psi|^2 \right) = 0 \; . \tag{1}$$

g is the coupling constant of the system and determines the "strength" of the non-linear character of the equation. Especially, as can be seen from the derivation of the modified non-linear Schrödinger equation from the discrete equations [10], the mass of the carbon atom is encoded into g.

III. EQUATION ON THE SPHERE

In this section, we will discuss the equation (1) above on a 2-dimensional sphere of radius R_s aiming to describe "electronic" excitations on fullerenes and fullerides.

5

The Laplacian operator in this case reads:

$$\Delta_{sphere} = \frac{1}{R_s^2} \left(\frac{\partial^2}{\partial \theta^2} + \cot \theta \frac{\partial}{\partial \theta} + \frac{1}{\sin^2 \theta} \frac{\partial^2}{\partial \varphi^2} \right) , \tag{2}$$

where $\theta \epsilon [0 : \pi]$ and $\varphi \epsilon [0 : 2\pi]$. Note that $\psi = \psi(t, \theta, \varphi)$ is a complex valued scalar field.

Solutions of (1) considered on the sphere with radius R_s can be characterised by their norm:

$$\eta^2 = \int_0^{2\pi} \int_0^{\pi} |\psi|^2 \sin \theta d\theta d\varphi \tag{3}$$

as well as by their energy:

$$E = \int_0^{2\pi} \int_0^{\pi} \left(|\vec{\nabla}\psi|^2 - 2g|\psi|^4 + \frac{1}{4}g(\vec{\nabla}|\psi|^2)^2 \right) \sin \theta d\theta d\varphi . \tag{4}$$

We will construct normalised solutions, i.e. $\eta^2 = 1$. Note that in [14] a different strategy was employed. By rescaling the wave-function $\psi \to \psi/\sqrt{g}$, the coupling constant g can be eliminated from the equation. (Of course, the normalisation of the wave-function is lost in this approach, but since η was plotted, the corresponding value of g could be easily determined.) In this paper, we put the emphasis on the evolution of the spectrum (corresponding to normalised eigenfunctions) as a function of the coupling constant g. Note that g determines the "strength" of the non-linear part of the equation and that for $g = 0$, the equation becomes the ordinary Schrödinger equation on the sphere, which, of course, is linear.

A. Discussion of the solutions

To construct explicit solutions, we employ the following axially symmetric Ansatz [15, 16]:

$$\psi(t, \theta, \varphi) = e^{-i\omega t + im\varphi} \Phi(\theta) . \tag{5}$$

The solutions with $m = 0$ are non-spinning solutions, while the spinning solutions will have $m \neq 0$.

Inserting this Ansatz into (1), we find the following equation [14]:

$$\Phi'' + \cot \theta \Phi' + \Phi'^2 \frac{g\Phi}{1 + g\Phi^2} + \frac{4g\Phi^3 + \omega\Phi}{1 + g\Phi^2} R_s^2 - \frac{m^2}{1 + g\Phi^2} \frac{1}{\sin^2 \theta} \Phi = 0 , \tag{6}$$

where the prime denotes the derivative with respect to θ.

This is a priori a non-linear equation with external parameters g and ω. Here, we will consider it from a slightly different point of view. Let us rewrite (6) as follows:

$$- \left(\Phi'' + \cot\theta \, \Phi' + \Phi'^2 \frac{g\Phi}{1+g\Phi^2} + \frac{g\Phi^3 R_s^2 (4-\omega)}{1+g\Phi^2} - \frac{m^2}{1+g\Phi^2}\frac{1}{\sin^2\theta}\Phi \right) = \Omega\Phi \qquad (7)$$

where

$$\Omega \equiv \omega R_s^2 \qquad (8)$$

is the effective spectral parameter. The equation then appears as an eigenvalue Schödinger equation supplemented by a non-linear term coupled with the parameter g. The solutions in the linear case, i.e. for $g = 0$ are well-known and it is very likely that - by continuity- their deformation due to the non-linear term can be constructed at least for small values of g. However, this does not exclude the occurence of supplementary branches of solutions, which may appear typically due to the non-linear structure of the equation.

In order to construct regular solutions, (7) has to be solved subject to the following boundary conditions:

$$\Phi'|_{\theta=0} = \Phi'|_{\theta=\pi} = 0 \quad \text{for} \quad m = 0 \qquad (9)$$

and

$$\Phi(\theta = 0) = \Phi(\theta = \pi) = 0 \quad \text{for} \quad m \neq 0 . \qquad (10)$$

To solve the equation (7) numerically subject to the boundary conditions (9), respectively (10) for generic values of g and R_s, we use a numerical routine based on the Newton-Raphson method [17]. Our strategy is to use $\Phi(\theta = 0)$, respectively $\Phi'|_{\theta=0}$ as a "shooting" parameter for the case $m = 0$ and $m \neq 0$.

1. The case $g = 0$

In the case $g = 0$, (7) reduces to the well-known Legendre equation

$$\Phi'' + \cot\theta \, \Phi' - m^2 \frac{1}{\sin^2\theta}\Phi + \Omega\Phi = 0 . \qquad (11)$$

The solutions of this equation are the associated Legendre functions:

$$\Phi(\theta) = P_l^m(\cos\theta) \quad \text{with} \quad \Omega = l(l+1) , \qquad (12)$$

where

$$l \in \mathbb{N} , \quad m = -l, -l+1, ..., l-1, l . \qquad (13)$$

The spatial part of (5) are then the spherical harmonics $Y_m^l(\theta, \varphi) = e^{im\varphi} P_m^l(\cos\theta)$. Notice, however, that in the equation studied here there is no distinction between m and $-m$. From now on, we will assume m to be positive, but it is understood that the solution with corresponding $-m$ can be trivially obtained.

The spherical harmonics have a well-defined parity, i.e. they are either symmetric or anti-symmetric under the reflection $\Phi(\theta) \to \Phi(\pi - \theta)$. In addition, the number of zeros in the interval $]0 : \pi[$ is equal to $l - |m|$.

These results are, of course, very well-known, but we mention them for completeness and because the spectrum of the full equation will approach the spectrum of the Legendre equation in the $g \to 0$ limit.

2. Deformed Legendre functions

All the solutions discussed in the previous section are continuously deformed when the parameter g is chosen to be larger than zero. For every available spherical harmonic, we observe that a branch of solutions in g exists, on which the solutions have the same symmetry than in the $g = 0$ limit. Our numerical results further indicate that the number of zeros k of the solution is preserved all along the branch and is equal to $k \equiv l - m$.

Now, we will discuss in detail the numerical solutions corresponding to the deformations of the spherical harmonics Y_0^0, Y_0^1 and Y_1^1.

- The non-spinning ($m = 0$) and nodeless ($l = 0$, $k = 0$) solution corresponding to the case Y_0^0 is in fact the constant solution of the equation, namely

$$\Phi = \sqrt{\frac{-\omega}{4g}} \ . \tag{14}$$

  The eigenvalue Ω of the corresponding normalised solution has a linear dependence of the parameter g:

$$\Omega = -\frac{R_s^2 g}{\pi} \ . \tag{15}$$

  This dependence is shown in Fig.1 for $R_s = 2$.

- The non-spinning ($m = 0$), one-node ($l = 1$, $k = 1$) solution is anti-symmetric under the reflection $\theta \to \pi - \theta$. The function $Y_0^1 \propto \cos\theta$ is progressively deformed by the non-linear term for $g > 0$. For $g \approx 10$ the profile of the function $\Phi(\theta)$ possesses

8

a plateau $\Phi = 0$ surrounding the region of $\theta = \pi/2$. Away from this plateau, the solutions resemble two disconnected solitons located at the two poles of the sphere, i.e. the maxima of $\Phi^2(\theta)$ are situated around $\theta = \pi$ and $\theta = 0$. Stated in other words, the probability density vanishes in a region surrounding the equator, while it has local maxima at the two poles. Let us stress, that the physical parameters remain monotonic functions of the "shooting" parameter $\Phi(\theta = 0)$.

The dependence of Ω on g is shown in Fig.1 for $R_s = 2$. For $g = 0$, we have $\Omega = 2$, as expected. It is worth noticing that the two eigenvalues corresponding to the quantum numbers $m = l = 0$ and $m = 0$, $l = 1$ cross at $g \approx 1.5$. This would a priori mean, that the "excited" solution becomes the "ground state" of the equation. However, as we will see in the next section, the appearance of new asymmetric solutions will turn out to have even lower values of Ω.

- The spinning ($m = 1$), no-node ($l = 1$, $k = 0$) solutions arrive as deformations of the spherical harmonic $Y_1^1 \propto \sin\theta e^{i\varphi}$. This solution is thus symmetric under the reflection $\theta \to \pi - \theta$. In contrast to the non-spinning solutions, we notice here that when the coupling constant g is of order 2.5, the structure of the solutions becomes very sensitive to the value of the "shooting" parameter $\Phi'|_{\theta=0}$. In other words, there exists a critical value of $\Phi'|_{\theta=0} \equiv \Phi'_{(cr)}|_{\theta=0}$ (depending on R_s) such that no solutions exist for $\Phi'|_{\theta=0} > \Phi'_{(cr)}|_{\theta=0}$. Our numerical results, however, suggest that solutions of arbitrary large values of g can be constructed when considering the limit $\Phi'|_{\theta=0} \to \Phi'_{(cr)}|_{\theta=0}$. The corresponding eigenvalue of Ω decreases monotonically with g from $\Omega = 2$ (for the case $g = 0$) as can be seen in Fig.1 for the case $R_s = 2$. Of course, this curve also represents the solution with $m = -1$, so that the eigenvalue Ω is three-fold degenerated in the limit $g = 0$.

Finally, let us state that for these solutions, the function Φ has a maximum at the equator and vanishes at the poles. This is an interesting result with view to [18]. In this latter paper it was found that if a C_{60} or a C_{70} molecule is doped with one or two excess electrons, the additional charges accumulate nearly along an equatorial line of the molecule.

Of course, deformations of the Legendre functions for higher m and l can be constructed in a systematic way.

3. Asymmetric solutions

All solutions of the non-linear equation (7) discussed previously appear as continuous deformations of the solutions available in the linear limit $g = 0$. However, in this section, we will exhibit new branches of solutions, which are fundamentally non-linear phenomena and as these have no linear counterparts. Numerically, we find that these new branches of solutions exist for sufficiently high values of the coupling constant g parametrising the non-linear effect and that some of these branches bifurcate into the branches of the deformed Legendre functions at critical values of $g = g_{cr}^{(m,l)}(R_s)$, which depend on l, m (and thus on the number of nodes $k = l - m$) as well as on the radius R_s.

These solutions are charaterised by the fact that they are asymmetric with respect to the reflection $\theta \to \pi - \theta$.

- Asymmetric, non-spinning ($m = 0$) and nodeless ($l = 0$, $k = 0$) solutions exist for $g > g_{cr}^{(0,0)}(R_s = 2) \approx 0.838$. When the parameter g is chosen larger than this critical value, our numerical results indicate that this solution has a maximum at $\theta = 0$ and a minimum at $\theta = \pi$ and decreases monotonically between these two extrema, which are strictly positive. Thus, the solution is neither symmetric nor anti-symmetric under the reflection $\theta \to \pi - \theta$. Instead, this reflection applied to the solution leads to an equivalent solution with a maximum (respectively minimum) at $\theta = \pi$ ($\theta = 0$). The solutions thus represent a physical state with probability density concentrated in one of the hemispheres. This is a new feature that cannot arise in the deformation of the Legendre functions.

In the limit $g \to g_{cr}^{(0,0)}$ the values of the maximum and the minimum approach each other and the solution becomes constant. The branch of these asymmetric solutions bifurcates into the branch of constant solutions (deformed Y_0^0) described in the previous section. The corresponding value of ω of these asymmetric solutions is lower than the one of the symmetric branch. This is shown in Fig.1 (dotted line) for $R_s = 2$.

For generic values of R_s, the bifurcation of the asymmetric branch occurs at

$$g_{cr}^{(0,0)}(R_s) = \frac{\pi}{R_s^2 - \frac{1}{4}} \quad , \tag{16}$$

with

$$\Omega_{cr}^{(0,0)} = -\frac{R_s^2}{R_s^2 - 1/4} \quad . \tag{17}$$

10

- Asymmetric, non-spinning ($m = 0$) and one-node ($l = 1$, $k = 1$) solutions exist for $g > g_{cr}^{(0,1)}(R_s = 2) \approx 25$. In this region of parameter values, we find that in fact two branches of solutions exist (see Fig.1). For a fixed value of g, the solution with the lower value of Ω has a bigger value of $\Phi(0)$ and its minimum lies at smaller values of θ. This is demonstrated for $g = 37$, $R_s = 2$ in Fig.2. The values of ω corresponding to these asymmetric solutions are higher than the values of the corresponding (i.e. with for the same values of g) antisymmetric solution on the branch of deformed Legendre functions Y_0^1. In contrast to the other described cases, we have not succeeded to construct another (a third) branch which would eventually bifurcate from the branch of deformed Legendre functions.

- Asymmetric, spinning ($m = 1$) and nodeless ($l = 1$, $k = 0$) solutions exist for $g > g_{cr}^{(1,1)}(R_s = 2) \approx 3.79$. Solving the equations for values of g larger than this critical value, we were able to construct a branch of asymmetric solutions (and the corresponding mirror symmetric one). The maximum of these solutions is located between $\theta = 0$ and $\theta = \pi/2$ such that the probability density is located in one of the hemispheres. As before, the frequency of the asymmetric solution is lower than the frequency of the corresponding (i.e. same g) solution on the deformed Y_1^1 branch.

The construction of asymmetric branches with higher values of the spin m and/or higher node numbers k becomes very tricky. This is mainly due to the occurence of many solutions existing for the same values of the parameters and also due to the fact that the profiles of the symmetric and asymmetric (or anti-symmetric and asymmetric) solutions can be very close to each other on a large part of the $[0 : \pi]$ interval. The construction of asymmetric branches can thus not be achieved systematically.

IV.   EQUATION ON THE DISC

In [13] the equation (1) was discussed on a two-dimensional plane and non-spinning as well as spinning solutions with nodes were constructed. Here, we will treat this problem differently. With view to the discussion of the equation on a sphere, we will discuss here the equation on a two-dimensional disc with radius R_d parametrized by the coordinates ρ and

φ. The case studied in [13] then arises as limit $R_d \to \infty$. The Laplacian is given by:

$$\Delta_{disc} = \frac{\partial^2}{\partial \rho^2} + \frac{1}{\rho} \frac{\partial}{\partial \rho} + \frac{1}{\rho^2} \frac{\partial^2}{\partial \varphi^2} \tag{18}$$

with $\varphi \in [0 : 2\pi]$. The norm reads:

$$\eta^2 = \int\limits_0^{2\pi} \int\limits_0^{R_d} |\psi|^2 \rho d\rho d\varphi \tag{19}$$

and the energy is given by:

$$E = \int\limits_0^{2\pi} \int\limits_0^{R_d} \left(|\vec{\nabla}\psi|^2 - 2g|\psi|^4 + \frac{1}{4} g(\vec{\nabla}|\psi|^2)^2 \right) \rho d\rho d\varphi . \tag{20}$$

A. Discussion of the solutions

As for the case on the sphere, we adopt the following Ansatz for the complex valued function $\psi(t, \rho, \varphi)$:

$$\psi(t, \rho, \varphi) = e^{-i\omega t + im\varphi} \phi(\rho) . \tag{21}$$

Inserting this Ansatz gives the following equation:

$$\phi'' + \frac{\phi'}{\rho} + \frac{g\phi\phi'^2}{1 + g\phi^2} + \frac{4g\phi^3 + \omega\phi}{1 + g\phi^2} - \frac{m^2\phi}{\rho^2(1 + g\phi^2)} = 0 , \tag{22}$$

where the prime now denotes the derivative with respect to ρ.

We can rewrite, analogue to before, the equation in the following way:

$$- \left(\phi'' + \frac{\phi'}{\rho} + \frac{g\phi\phi'^2}{1 + g\phi^2} + \frac{g\phi^3(4 - \omega)}{1 + g\phi^2} - \frac{m^2\phi}{\rho^2(1 + g\phi^2)} \right) = \omega\phi . \tag{23}$$

This equation looks like the one studied in [13], however, we impose different boundary conditions here:

$$\partial_\rho \phi|_{\rho=0} = 0 \ , \quad \phi(R_d) = 0 \quad \text{for} \quad m = 0 \tag{24}$$

and

$$\phi(\rho = 0) = 0 \ , \quad \phi(R_d) = 0 \quad \text{for} \quad m \neq 0 . \tag{25}$$

Again, we used the numerical routine described in [17] to solve the equation (23) subject to the boundary conditions (24), respectively (25).

12

1. The g = 0 limit

In the limit $g = 0$ (23) reduces to the linear Schrödinger equation in polar coordinates

$$\phi'' + \frac{\phi'}{\rho} - \frac{m^2\phi}{\rho^2} + \omega\phi = 0 \ . \tag{26}$$

Note that for static solutions, i.e. $\omega = 0$, the equation reduces to the Euler equation with solutions of the form $\psi(t, \rho, \varphi) \equiv \psi(\rho) \propto e^{im\varphi}\rho^m$. For $\omega \neq 0$, the equation becomes the Bessel equation if we define $x \equiv \sqrt{|\omega|}\rho$ and $F(x) \equiv \phi(x)$:

$$\frac{d^2F}{dx^2} + \frac{1}{x}\frac{dF}{dx} + \left(1 - \frac{m^2}{x^2}\right)F = 0 \tag{27}$$

The solutions of this equation, which are regular at the origin are of course the well-known Bessel functions $J_m(x)$ for $\omega > 0$ and the modified Bessel functions $I_m(x)$ for $\omega < 0$. Remembering that the Bessel functions $J_m(x)$ are oscillating and admit an infinite number of nodes on the positive real axis, it is easy to construct solutions of (26) with k nodes. This is possible assuming that

$$\phi(\rho) = J_m(\sqrt{\omega}\rho) \ \ \text{with} \ \ \phi(R_d) = 0 \tag{28}$$

and choosing the value of ω in such the way that the value $\rho = R_d$ coincides with the k-th zero (we call it $x = x_{m,k}$) of the Bessel function J_m, i.e. $\sqrt{\omega} = x_{m,k}/R_d$.

This indicates that in the limit $g = 0$ solutions with angular momentum m and with k nodes exist and the spectrum of the equation is positive. The corresponding functions are convex.

2. The g ≠ 0 case

If the coupling constant g is positive but small, we expect that the pattern of solutions will be similar to the one available in the limit $g = 0$ discussed above. Our numerical results indeed confirm this expectation. For small values of g, the solutions are still represented by convex functions and the values of ω are positive and decrease slowly with g as shown in Fig. 3 for the case $m = 0$, $k = 0$. Let is call this range of g-values the "weak coupling-regime".

When g is large enough, the value of ω becomes negative (see Fig.3) and the solutions have an inflexion point at some intermediate value of ρ (see Fig.4). As a consequence they

become much more localized in the region around the origin. In this "strong coupling-regime" the solutions can thus be described as being soliton-like. We also note that the value of ω decreases very strongly with g.

The difference between the strong and weak coupling is shown in Fig.4 for $g = 1$, respectively $g = 8$ and $R_d = 5$. The value ω is shown in dependence on g for the non-spinning ($m = 0$) and nodeless ($k = 0$) solution for different values of the disc-radius R_d in Fig.3.

In Fig. 3 we also superposed the values of ω corresponding to the case of the full plane (i.e. $R_d = \infty$). As has been shown in [10, 13], in this case, solutions exists only for large enough values of g: $g \geq g_{cr} \approx 2.94$. It is therefore natural to try to understand the pattern available on the plane as the $R_d \to \infty$ limit of the pattern of solutions for the disc. In this respect, it is interesting to notice that in the "strong coupling-regime" the values of ω corresponding to a finite disc get very close (especially for the case corresponding to $R_d = 10$) to the values of ω associated with the case of the infinite disc. This is related to the fact that with increasing g, the "soliton" becomes more and more peaked around the origin and doesn't "notice" whether the disc is finite or infinite. This observation gives a natural explanation for the fact that solutions exist only for $g \geq g_{cr}$ in the case of the plane. Indeed in the case of the plane, it was noticed [13] that the linearized equation (valid asymptotically) also is of Bessel type. However, the nodeless, localized solutions are exponentially decreasing and can only be associated with the modified Bessel function, which correspond to negative values of ω. That's why, on the plane, nodeless soliton-like solutions exist only for $g \geq 2.94$ and have no "weak coupling"-counterparts. For large values of g the numerical results strongly suggest the following linear relation between g and the frequency corresponding to the fundamental mode : $\omega \approx -0.66g + 2.19$. We also studied the solutions with $k > 0$ nodes and $m > 0$ and found that the pattern is similar to the case $k = 0$ and $m = 0$ discussed above in detail.

We do not find it useful to discuss them here, but we believe that our results provide a robust evidence that regular solutions of (23) with an arbitrary number of nodes and arbitrary (integer) angular momentum exist on the disc/plane.

V.   EQUATION ON THE CYLINDER

We also considered the equation on a cylinder of radius R_c and length $2L$. This is a natural extension of the previous results in order to describe soliton-like structures on nanotubes

with radius R_c and length $2L$. Using the natural coordinates z, φ, the Laplacian reads:

$$\Delta_{cylinder} = \frac{1}{R_c^2}\frac{\partial^2}{\partial\varphi^2} + \frac{\partial^2}{\partial z^2} \tag{29}$$

with $\varphi \in [0 : 2\pi]$ and $z \in [-L, L]$. The norm reads:

$$\eta^2 = \int\limits_{0}^{2\pi}\int\limits_{-L}^{L} |\psi|^2 dz d\varphi \tag{30}$$

and the energy is given by:

$$E = \int\limits_{0}^{2\pi}\int\limits_{-L}^{L} \left(|\vec{\nabla}\psi|^2 - 2g|\psi|^4 + \frac{1}{4}g(\vec{\nabla}|\psi|^2)^2 \right) dz d\varphi \ . \tag{31}$$

A. Discussion of the solutions

We use the following Ansatz:

$$\psi(t, z, \varphi) = e^{-i\omega t + im\varphi} F(z) \ , \quad m = 0, 1, 2, \ldots \tag{32}$$

The equation (1) then becomes:

$$F'' + (F')^2\frac{gF}{1 + gF^2} + \left(4gF^2 + \omega - \frac{m^2}{R_c^2} \right)\frac{F}{1 + gF^2} = 0 \ , \tag{33}$$

where the prime denotes the derivative with respect to z.

Again, we can rewrite this equation in terms of a "spectral equation":

$$- \left[F'' + (F')^2\frac{gF}{1 + gF^2} + \left(gF^2(4 - \omega) - \frac{m^2}{R_c^2} \right)\frac{F}{1 + gF^2} \right] = \omega F \ . \tag{34}$$

This equation has to be solved subject to the following boundary conditions:

$$F(-L) = F(L) = 0 \ . \tag{35}$$

The equation (33) is then solved subject to the boundary conditions (35) using the numerical routine described in [17].

1. The case $g = 0$

The case $g = 0$ corresponds to an harmonic equation:

$$F'' = -\left(\omega - \frac{m^2}{R_c^2} \right) F \ . \tag{36}$$

The solutions of this equation subject to the boundary conditions (35) are:

$$F(z) = \sin\left((z-L)\sqrt{\omega - m^2/R_c^2}\right) \quad \text{with} \quad \omega = \left(\frac{m}{R_c}\right)^2 + \left(\frac{\pi n}{2L}\right)^2 \quad, \quad n = 1, 2, 3, \ldots \quad (37)$$

B.   The case $g \neq 0$

It is possible to solve (33) by quadrature, which gives:

$$(F')^2 = \frac{C - 2gF^4 - \Omega F^2}{1 + gF^2} \quad, \quad \Omega \equiv \omega - \frac{m^2}{R_c^2} \tag{38}$$

and C is an integration constant. The integration can be performed, however, it leads to an involved and untractable expression of z in terms of F, C, Ω. Assuming the cylinder to be infinite ($L = \infty$) and $F(\infty) = F'(\infty) = 0$ leads to $C = 0$. If we now require in addition that the solution is symmetric under the reflexion $z \to -z$ (i.e. $F'(0) = 0$) we obtain the relation $\Omega = -2gF(0)^2$. This provides a useful check for our numerical results.

Performing a numerical analysis of the values of ω as a function of g (with L, R_c, k, m fixed), we obtain a pattern very similar to that available for the case on a disc (see Fig.3). The only noticable difference resides in the fact that, in the limit $L = \infty$, a normalizable solution can be constructed for all values of the parameter g. This case is, of course, interesting with iew to nanotubes since the lengths $2L$ of a tube is much larger than its diameter $2R_c$. In the case of the "ground state" solution, which is non-spinning ($m = 0$) and nodeless ($k = 0$), the following relations hold :

$$\omega \approx -0.1g^2 \text{ for } g \ll 1 \quad, \quad \omega \approx -0.555g + 1.28 \text{ for } g \gg 1 \,. \tag{39}$$

Unlike in the case of the sphere, we did not succeed in constructing asymmetric solutions in the case of the cylinder (i.e. solutions, which are neither even nor odd under the reflexion $z \to -z$) and we believe that there are no such solutions.

$$(40)$$

VI.   CONCLUSIONS

In this paper we have presented an extended analysis of a modified non-linear Schrödinger equation in 1+2 dimensions. This equation was constructed as an effective continuous

equation describing an interaction of an excitation with a 2-dimensional hexagonal lattice. In this paper, we think of the excitation as an "excess electron" described by a wave function ψ and the interaction to be "electron-phonon" -like. As is well-known from amide I-excitations in biopolymeric lattices such an interaction leads to the creation of a localised state, a "soliton".

The continuous modified non-linear Schrödinger equation was obtained with the idea to approximate the physical system on the plane [10, 13], but it can be modified in order to be considered on different geometrical manifolds, which are justified physically. These are, namely, a cylinder to mimick excitations on a carbon nanotube and a sphere, respectively, in order to describe excitations (e.g. extra electrons) on a fullerene nanomolecule, which is particularly interesting with view to the possibility of describing the high transition temperature of superconducting fullerides.

Completed with the different types of boundary conditions related to the geometry and using an Ansatz previously introduced in the study of boson stars [15] and spinnning Q-balls [16], the equation (1) possesses a lot symmetries, some are continuous (like rotations), some are discrete (like reflexions).

In all cases considered the spectrum of solutions is rich, many "normal-mode"-types of solutions exist, mainly characterized by two integers: the internal angular momentum (or spin) and the number of nodes of the wave function. This is very reminiscent to the principal quantum numbers of more familiar quantum mechanical systems.

It might turn out to be difficult to classify the solutions of a non-linear, partial differential equations. The various types of solutions, however, can be traced back from the corresponding solutions available in the weak coupling limit, in which the equation becomes linear and its spectrum is known analytically. In the case of the sphere, disc and cylinder, respectively, we found deformed Legendre functions, deformed Bessel functions and deformed harmonic functions. However, in the case of the sphere, we demonstrated the existence of additional solutions, which are specifically related to the non-linear character of the equation. The main feature distinguishing these supplementary solutions is their asymmetry with respect to the reflexion at the equator of the sphere. In other words, we exhibited the spontaneous symmetry breaking (SSB) of one of the natural symmetries of the initial problem.

This SSB occurs when the non-linear coupling becomes strong enough. Similarly it can occur for very different types of non-linear equations. As an example, we point out the

bifurcation of bisphaleron solutions from the sphaleron solutions available in the case of the classical equations of the electroweak field theory [19, 20]. In this case, the parity operator is spontaneously broken by the so called bisphaleron solutions.

---

[1] H. W. Kroto, J. R. Heath, S. C. O'Brien, R. F. Curl and R. E. Smalley, Nature **318** (1985), 162.

[2] R. C. Haddon *et al.*, Nature **350** (1991), 320; *for a review see* O. Gunnarsson, Rev. Mod. Phys. **69** (1997), 575.

[3] K. Tanigaki, T. W. Ebbesen, S. Saito, J. Mizuki, J. S. Tsai, Y. Kubo and S. Kuroshima, Nature **352** (1991), 222.

[4] C. M. Varma, J. Zaanen and K. Raghavaclari, Science **254** (1991), 989; M. A. Schluter, M. Lannoo, M. Needles, G. A. Baraff and D. Tomanek, Phys. Rev. Lett. **68** (1992), 526; J. Phys. Chem. Solids **53** (1992), 1473; I. I. Mazin, S. N. Rashkeev, V. P. Antropov, O. Jepsen, A. I. Lichtenstein anbd O.K. Andersen, Phys. Rev. **B45** (1992), 5114.

[5] S. Iijima, Nature (London) **354** (1991), 56.

[6] S. Iijima and T. Ichihashi, Nature (London), **363** (1993), 603.

[7] see e.g. M. S. Dresselhaus, G. Dresselhaus and P. Eklund, *The Science of fullerenes and carbon nanotubes* (Academic, New York, 1996); *Carbon nanotubes, Preparation and Properties*, edited by T. W. Ebbesen (CRC, Boca Raton, FL, 1996); R. Saito, G. Dresselhaus and M. S. Dresselhaus, *Physical Properties of carbon nanotubes* (World Scientific, Singapore, 1998); P. J. F. Harris, *Carbon Nanotubes and Related Structures* (Cambridge University Press, Cambridge, 1999); *Carbon nanotubes: Synthesis, Structure, Properties and Applications*, edited by M. S. Dresselhaus, G. Dresselhaus and P. Avouris (Springer Verlag, Berlin, 2000).

[8] A. S. Davydov, *Solitons in Molecular systems* (Reidel, Dordrecht, 1985).

[9] A. Scott, Phys. Rep. **217** (1992), 1; *Nonlinear excitations in Biomolecules*, edited by M. Peyrard (Springer, Berlin, 1996).

[10] B. Hartmann and W. J. Zakrzewski, Phys. Rev. **B 68** (2003), 184302.

[11] L. Brizhik, A. Eremko, B. Piette and W. J. Zakrzewski, Physica **D 146** (2000), 275; **D 159** (2001), 71.

[12] L. Brizhik, B. Piette and W. J. Zakrzewski, Ukr. Fiz. Zh. (Russ. Ed.) **46** (2001), 503.

[13] Y. Brihaye, B. Hartmann and W. J. Zakrzewski, Phys. Rev. **D 69** (2004), 087701.

[14] Y. Brihaye and B. Hartmann, J. Phys. **A 37** (2004), 1181.

[15] F. E. Schunck and E. W. Mielke, in *Relativity and Scientific Computing*, Springer, Berlin (1996), 138.

[16] M. Volkov and E. Wöhnert, Phys. Rev. **D 66** (2002), 085003.

[17] U. Ascher, J. Christiansen and R. D. Russell, Math. Comput. **33**, (1979), 659; ACM Trans. Math. Softw. **7** (1981), 209.

[18] K. Harigaya, Phys. Rev. **B45** (1992), 13676.

[19] J. Kunz and Y. Brihaye, Phys. Lett. **B 216**, 353 (1989).

[20] L. G. Yaffe, Phys. Rev. **D 40**, 2723 (1989).
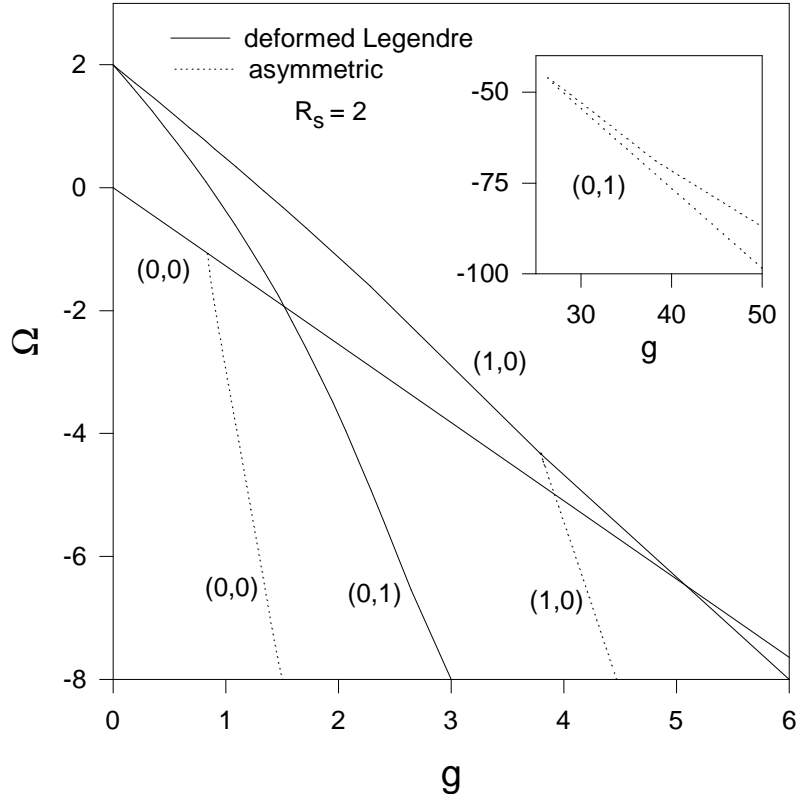
FIG. 1: The eigenvalue $\Omega = \omega R_s^2$ is shown as a function of g for $(m, l) = (0, 0)$, $(0, 1)$ and $(1, 0)$. We have chosen $R_s = 2$. The solid lines denote the deformed Legendre functions, while the dotted lines are the asymmetric solutions (see text for more details).
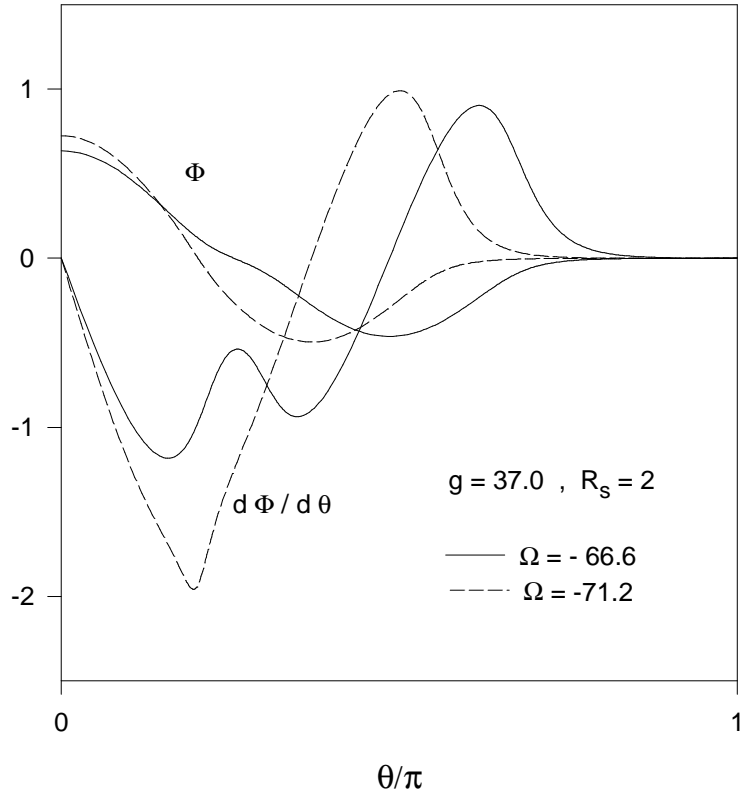
20

FIG. 2: The profiles of the function $\Phi(\theta)$ and the derivative $\frac{d\Phi}{d\theta}$ are shown for $(m, l) = (0, 1)$ (non-spinning, nodeless solutions), $g = 37$, sphere-radius $R_s = 2$ and two different values of the spectral parameter $\Omega = \omega R_s$.
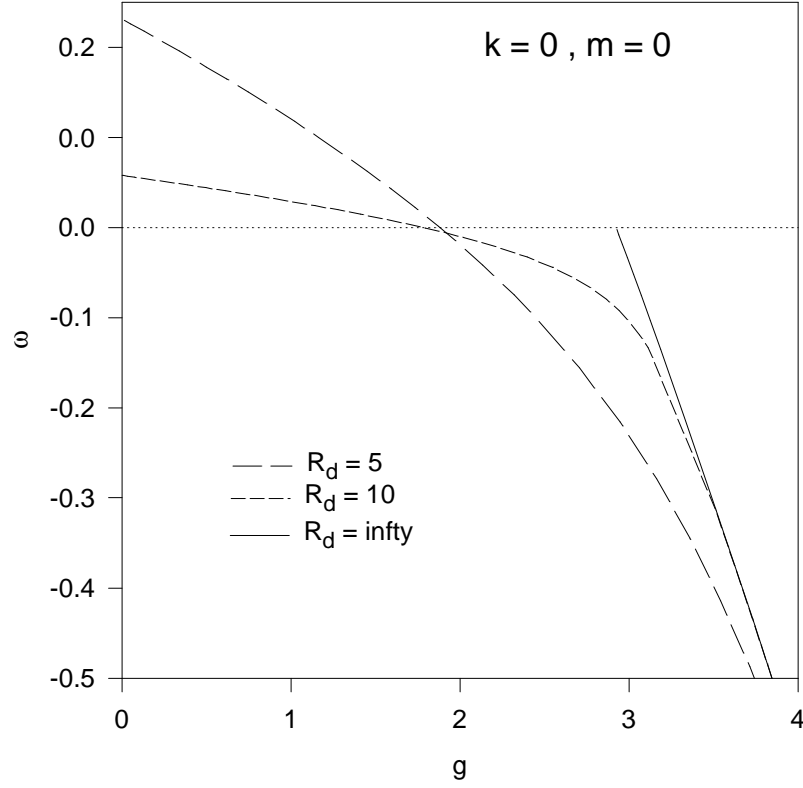
FIG. 3: The eigenvalue ω is shown as a function of g for the non-spinning $(m = 0)$, nodeless $(k = 0)$ solutions on the disc. We have chosen $R_d = 5$, 10 and ∞. Note that $R_d = \infty$ corresponds to the case of the plane.
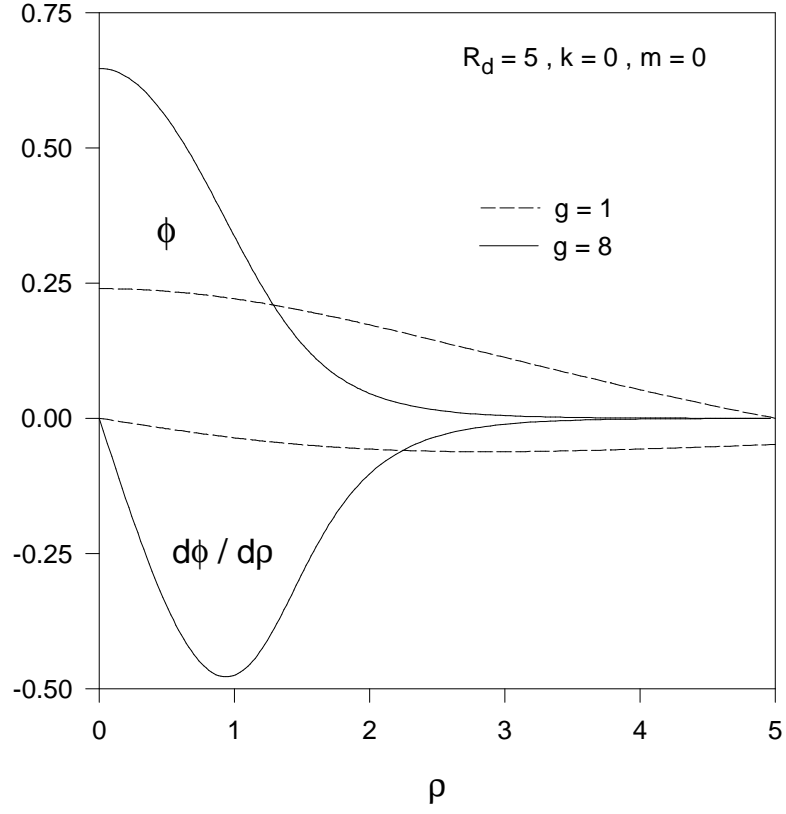
FIG. 4: The profiles of the function $\phi(\rho)$ and the derivative $\frac{d\phi}{d\rho}$ are shown for non-spinning $(m = 0)$, nodeless $(k = 0)$ solutions on the disc with radius $R_d = 5$ for two different values of g.